

Seismic response of steel braced frames equipped with shape memory alloy-based hybrid devices

Neda Salari and Behrouz Asgarian*

Faculty of Civil Engineering, K. N. Toosi University of Technology, Tehran, Iran

(Received May 15, 2014, Revised December 24, 2014, Accepted January 14, 2015)

Abstract. This paper highlights the role of innovative vibration control system based on two promising properties in a parallel configuration. Hybrid device consists of two main components; recentering wires of shape memory alloy (SMA) and steel pipe section as an energy dissipater element. This approach concentrates damage in the steel pipe and prevents the main structural members from yielding. By regulation of the main adjustable design parameter, an optimum performance of the device is obtained. The effectiveness of the device in passive control of structures is evaluated through nonlinear time history analyses of a five-story steel frame with and without the hybrid device. Comparing the results proves that the hybrid device has a considerable potential to mitigate the residual drift ratio, peak absolute acceleration and peak interstory drift of the structure.

Keywords: shape memory alloy; recentering capability; energy dissipater component; nonlinear time history analysis; structural control

1. Introduction

Current seismic design philosophy expects no significant damage to structural systems during low to moderate amplitude of earthquake and no collapse of structures during major earthquake. During strong excitations, structures are expected to experience inelastic range of deformation sustaining permanent residual deformations in primary lateral load-resisting elements, which can result in substantial losses such as repair, downtime costs and undesirable response of the structure to pursuant aftershocks. After the weak performance of moment-resisting frames in Northridge earthquake, extensive researches have been performed to decrease the problems of geometric nonlinearity and brittle fracture of welded beam-to-column connections for future events (Sabelli *et al.* 2003).

Ordinary steel braced frames have an appropriate performance in minor to moderate earthquakes. However, depends to the system properties, it has a poor performance during major earthquakes due to limited ductility, low energy dissipation, low cycle fatigue life and the asymmetric hysteresis behavior (Tremblay *et al.* 2003, Uriz and Mahin 2004). Hence, research works have been implemented to seek for concentric braced frames with better performance (Sabol 2004). Buckling Restrained Braced Frames (BRBFs) were innovated to overcome the buckling

*Corresponding author, Associate Professor, E-mail: asgarian@kntu.ac.ir

problem of conventional braces (Watanabe *et al.* 1988, Asgarian and Shokrgozar 2009). Although these systems own enhanced hysteretic behavior, they are susceptible to residual displacements after major earthquakes (Fahnestock *et al.* 2003, Uang and Kiggins 2003, Tremblay and Poncet 2004, Asgarian and Amirhesari 2007). So, other alternative methods have been recently conceived.

“Passive control” techniques utilize a wide range of materials and technologies to divert some of the input seismic energy to special devices such as supplemental fuse type dampers inserted in the structural systems (Constantinou *et al.* 1998, Tagawa and Gao 2012, Karavasilis *et al.* 2012). From this standpoint, the main structural system is intended to have little or no damage, whereas fundamental damages concentrate within accessible and easily replaceable substructures. Despite the slight increment in the initial design cost, considerable decrement in the heavy life-cycle cost associated with earthquake damage will occur (Wada 2010). The passive energy dissipation systems can be widely categorized into three types: (1) Visco-Elastic Devices; (2) Hysteretic Devices; (3) Dynamic Vibration Absorbers. In General, interstory drifts and subsequently stresses in primary members are decreased. However, all of the above mentioned systems have some intrinsic limitations such as problems related to servicing, ageing and durability, installation or substitution complexity and geometry restoration after extreme events (Dolce *et al.* 2000).

To eliminate these problems, modern energy dissipater systems have attracted considerable attention of scholars and designers. After the introduction of Shape Memory Alloys (SMAs) and their unique characteristics, they have received a growing interest for civil engineering applications (Janke *et al.* 2005, Song *et al.* 2006, Dolce and Cardone 2006, Asgarian and Moradi 2011). Their remarkable features are: high damping capacity, recentering properties, extraordinary corrosion resistance, high cycle fatigue life, great durability, no degradation due to ageing, no complexity of maintenance or replacement (even after major earthquakes), good control of forces, possibility to acquire an extensive range of cyclic behavior, limited encumbrance and functional simplicity (Dolce and Cardone 2001, DesRoches *et al.* 2004, Duerig *et al.* 1990, Miyazaki *et al.* 1986, Van Humbeeck 1991).

Hybrid control is an innovative idea with combining two sub-components into a configuration; these devices can aim at mitigating damage caused by earthquake and the associated cost (Marshall and Charney 2010). At present, SMA-based hybrid devices are one of the promising systems which are capable of increasing damping whilst minimizing displacements. Superelastic SMAs have shown a double flag-shape hysteresis under cyclic axial loading. With this aim, they could revert back to their original state which results in limited residual displacement of the structural system. Several studies have been reported on the performance of SMA-based devices (Karavasilis *et al.* 2011, Yang *et al.* 2010, Ozbulut and Hurlebaus 2011, Jalaeifar and Asgarian 2012). This paper proposes a new type of hybrid system which comprises of SMA wires and steel. The favorable concept behind the hybrid device is the parallel use of steel and SMA sub-components.

2. SMA based hybrid device

Steel materials have a ductile behavior; members with fully compact sections and proper lateral supports have the same properties and can be used as an energy absorption element of structure in major earthquakes. However, permanent displacement of energy dissipater devices made from steel elements will be high in strong earthquakes. In parallel, SMA has low energy absorption capability compared to steel elements; however, its unique recentering properties lead to combine

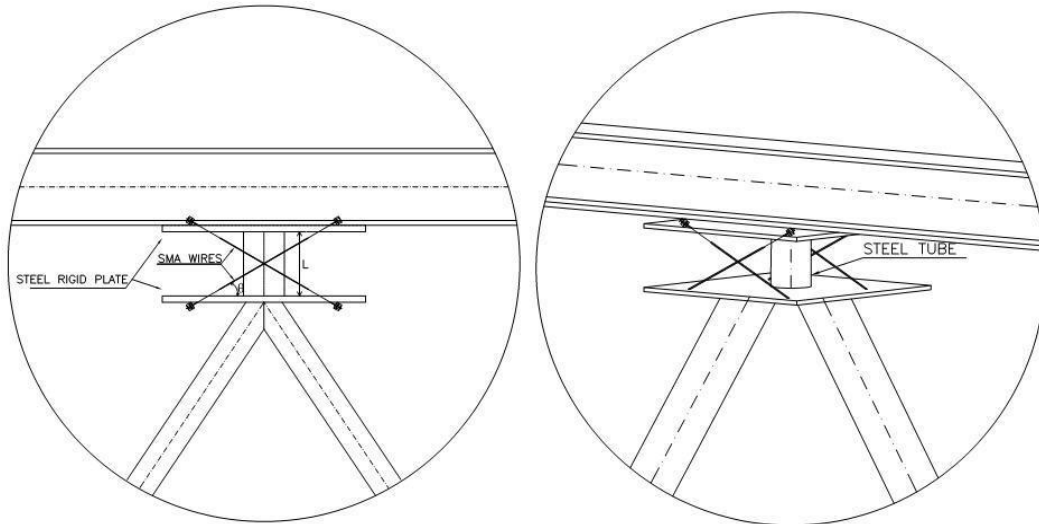


Fig. 1 Situation of hybrid device between beam and braces

it with steel elements to reach a hybrid device. By proper combination of steel and SMA elements, a hybrid device can be achieved having both energy absorption and recentering properties. The proposed hybrid device is composed of a steel pipe as an energy dissipater and two pairs of identical transverse NiTi wires as recentering components. In addition to two main components, two plates are installed at both ends for exerting boundary conditions. A mechanical configuration of the hybrid device is illustrated in Fig. 1. It should be mentioned that the hysteretic behavior of a hybrid device is produced by superposition of the superelastic behavior of SMA wire and yield effect of steel pipe. This device can be placed between the beam and top of a chevron brace configuration. During cyclic loading, when relative displacement is induced between the two plates, at any time, only NiTi wires in one direction are in tension; the wires in another direction are idle under compression. After that, the system returns to its initial zero load-zero deformation position in each cycle.

3. Numerical modeling of proposed hybrid device

In this section, after a summary review on shape memory alloys and mechanical properties of hybrid device elements, numerical modeling of proposed device is presented.

3.1 Overview of shape memory alloys

SMA's were discovered in 1932 but after 1962 they gained attention in comprehensive applied studies. At the macroscopic level, SMA's exist in two distinguished phases: the high temperature and low stress phase with a high symmetry known as austenite, whereas the low temperature and high stress phase with low symmetry is called martensite (Song *et al.* 2006). The austenite has a strong body-centered cubic crystal structure, while the martensite has a weak parallelogram structure. Moreover, SMA's undergo a unique transformation between two crystallographic phases.

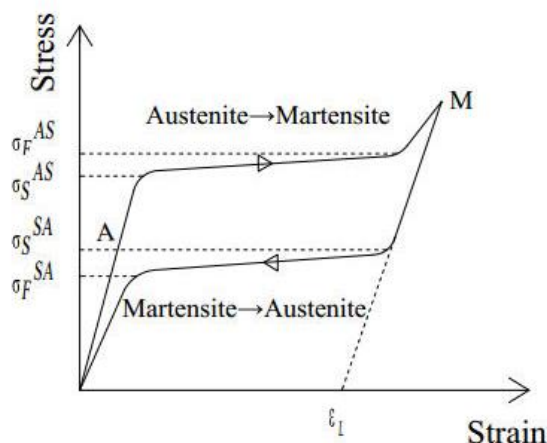


Fig. 2 Stress-strain relationship of superelastic SMA

The distinctive properties of SMAs are exactly due to a reversible thermal or stress-induced phase transformation. Superelastic Effect (SE) refers to the phenomenon of recovering large strains (up to 10 percent) after the removal of the load and Shape Memory Effect (SME) is the capability of regaining the initial configuration upon heating.

Fig. 2 shows a typical stress-induced transformation of the SMA which results in superelasticity. As shown in the figure, the stress-strain relationship of superelastic SMAs includes linear austenite, phase transformation and linear martensite (Motahari *et al.* 2007). σ_S^{AS} and σ_F^{AS} are the starting and finishing stresses in martensite forward transformation, respectively. Similarly σ_S^{SA} and σ_F^{SA} are the starting and finishing stresses in austenite reverse transformation, respectively. Besides, ε_L is the superelastic plateau strain length. At a temperature greater than austenite finish temperature, the SMA is in austenite phase. Due to loading, the phase transformation initiates and martensitic SMA is formed. When the applied load is removed, the martensite reaches its instability and therefore returns to austenite. In fact, this loop generates the flag-shape hysteresis (SE).

The transition temperatures depend on the alloy composition and thermal conditions. Experimental studies demonstrate that NiTi based alloys with near-equiatomic composition are the most practical SMAs in passive control of structures.

3.2 SMA wires modeling and verification

Due to the lack of the superelastic SMA material in the library of ABAQUS/Standard package (ABAQUS, version 6.5), stress-strain diagram was defined through FORTRAN programming and applied in the model by means of user material definition. It is very important to define the exact relations that encompass sudden unloading in each point of the path. Transformation stresses are derived from experimental study (Jalaeefar and Asgarian 2012). The exact composition is 53.5% and 46.5% for Ni and Ti, respectively. The test condition has been designed according to ASTM F2516-07, 'Standard Test Method for Tension Testing of Nickel-Titanium Superelastic Materials'. The tests have been conducted on SMA bar with a diameter of 8mm and length of 100mm. The mechanical properties of tested SMA are shown in Table 1.

Table 1 Mechanical properties of SMA (Jalaeefar and Asgarian 2012)

Quantity	Value
σ_F^{SA}	100 (MPa)
σ_S^{SA}	250 (MPa)
σ_S^{AS}	525 (MPa)
σ_F^{AS}	600 (MPa)
E^{SMA}	21500 (MPa)
ε_L	3%

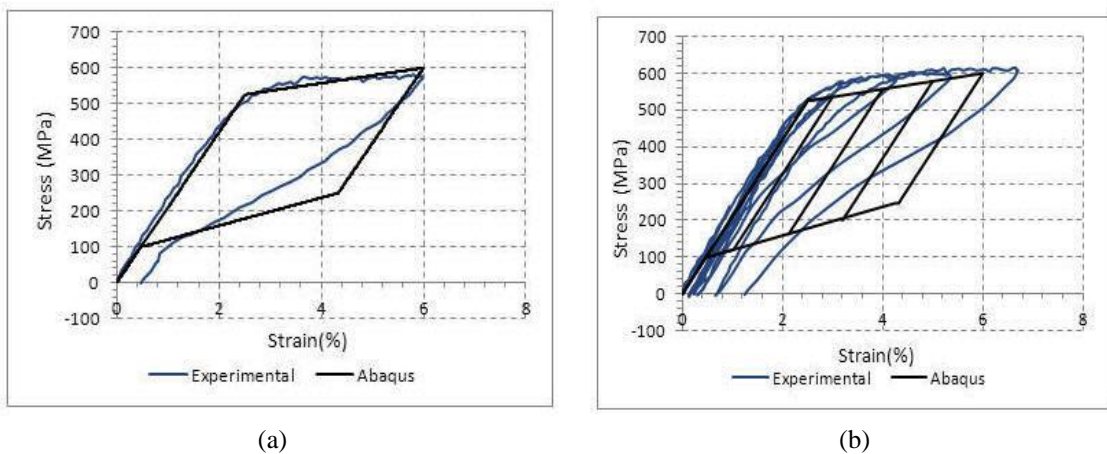


Fig. 3 Verification: stress-strain loops, Experimental data and numerical simulation (a) One cycle (b) Strain path (Jalaeefar and Asgarian, 2012)

It is assumed that SMA wires are susceptible to buckling under compressive loading. Therefore the stress-strain diagram of SMA is defined without considering the compression loop. Despite the ability of SMA to restore the high strains, a conservative value of 6% (corresponds to point M in Fig. 2) is adopted to prevent overloading of the adjacent components such as connections; this is an aftermath of SMA second hardening phenomenon. In addition, less than the strain of 6%, the fatigue life of SMAs can reach myriad load cycles of large displacement. By applying this safety margin, SMA wires can fully recover their initial shape without permanent deformation.

Fig. 3 presents the numerical SMA simulation results against the experimental ones. SMA is loaded under both one cycle and several cycles. The applied strain path is consisted of cycles of increasing strain amplitude of 1% to 6% by increments of 1% (Jalaeefar and Asgarian 2012). Figs. 3(a) and 3(b) illustrate the comparison between the experimental results and numerical simulation for SMA bar under one cycle and several cycles, respectively. The FE model regains its initial shape, whereas residual strain accumulates in the experimental sample, generally the results indicate that the FE model is in a good agreement with the experimental data. In spite of residual strain which remains in cyclic tests of SMA, a simplified model without strain accumulation is considered in most of the SMA engineering applications (Yang *et al.* 2010, Ozbulut and Hurlebaus 2011, Song *et al.* 2006).

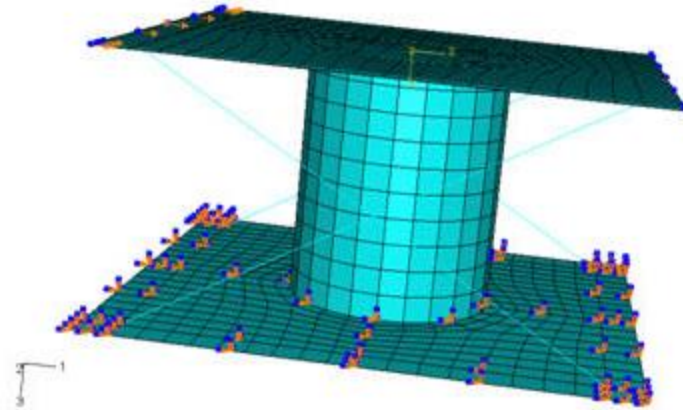


Fig. 4 Numerical model of the hybrid device

3.3 Modeling of SMA-based hybrid device

This section describes the numerical study of the hybrid device. Fig. 4 shows general configuration of the model. The boundary and support conditions are modeled by restricting all nodes of the bottom plate in all directions which means that the bottom plate is fixed. Load is applied in the form of displacement in the X-direction at the nodes of the left edge of the top plate.

Each wire composes of several SMA wires with sub-millimeter diameters to provide the required cross section. It is worth noting that by this means the complexity of machining associated with SMAs is eliminated. Analyses are carried out using ABAQUS finite element program. Shell element is applied for modeling of the steel pipe and plates. In order to model the material properties of the pipe section, the yield stress is assumed to be 250MPa , having Young modulus of $E=200\text{GPa}$. This is according to the material utilized for testing a pipe damper under cyclic shear (Maleki and Bagheri 2010). The formulation of $V_{SMA}=2F_{SMA}\cos\theta$ is applied to design the recentering component of the device; F_{SMA} is the axial load induced in the wires which dictates the cross-sectional area of the wires and θ is the inclination angle of the wires. Percentage of design load which is carried by SMA wires is named as “incorporation percentage of SMA”, in other words, it is defined as ratio between the horizontal component of SMA force and the summation of pipe shear force and horizontal component of SMA force; following expression can make it more sensible:

$$\frac{V_{SMA}}{P} = \text{Incorporation percentage of SMA, where } P = V_{SMA} + V_{pipe} .$$

Four design parameters are assessed to determine the device ideal performance; the design load, the incorporation percentage of SMA, height of the device and the inclination angle of the SMA wires. Parametric study is applied to determine the effect of these parameters on the device seismic performance, therefore, the behavior of 16 instances of the hybrid device have been investigated under cyclic loading to evaluate their workability; it is found that higher values for design loads, incorporation percentage of SMA and pipe lengths generally improve the objective workability. Conversely, increase in wire slope unfavorably affects the flag-shaped hysteresis loop of the device. Detailed results of the parametric study are not the main goal of this paper; however, one

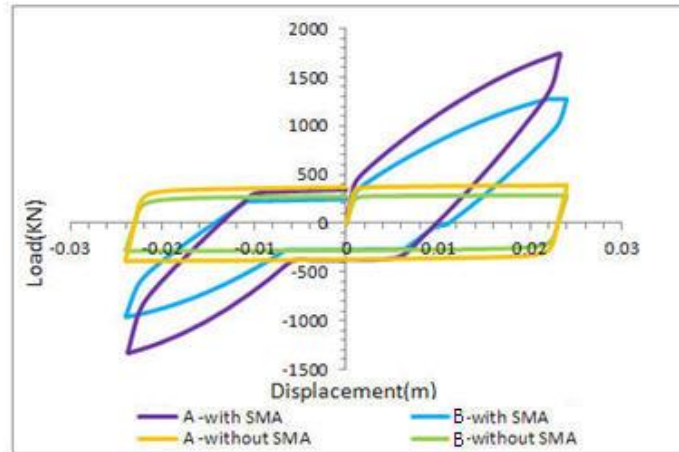


Fig. 5 Effect of design load on the device hysteresis loops

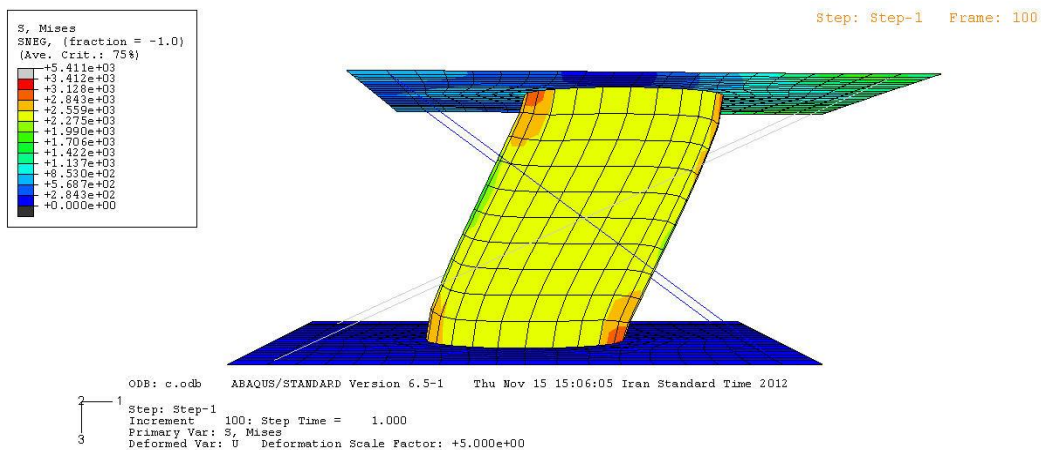


Fig. 6 Deformation of the device components under applied loading (scale factor=5)

of the sample cases which compares the effect of design load is illustrated in Fig. 5. The figure shows the juxtaposition of the curves with different values of design load, while other three parameters are constant. Case A is considered for higher level of design load than case B, for a better understanding of the effect of SMA wires on recentering performance, similar analyses were carried out on identical samples in the absence of the SMA wires. The outcome shows that the devices equipped with SMA wires are powerfully capable of reducing the residual displacements.

Fig. 6 depicts the relative displacement between two plates for one of the samples, for a better understanding, the deformed shape is shown with an amplification factor of five.

3.4 Optimum incorporation percentage of SMA

The incorporation percentage of SMA is one of the most considerable parameters on changing the hysteretic behavior of the hybrid device. The percentage of dissipated energy and recentering for cases with different incorporation of SMA are analyzed and the results are delineated in Fig. 7.

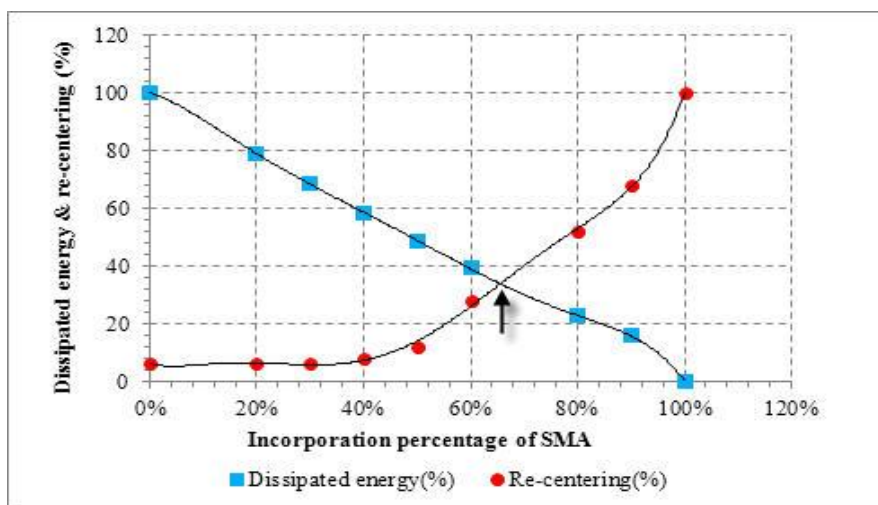


Fig. 7 Optimum incorporation percentage of SMA

It should be noted that the value of design load, pipe length and inclination angle of wires are constant in each point of the curves. For a better understanding, both values of dissipated energy and recentering are presented as percentage. Thus, dissipated energy is normalized to its maximum value. As can be seen, two curves follow inverse trends; the percentage of recovered displacement has a direct relationship with SMAs incorporation, whereas the amount of dissipated energy decreases by increasing the incorporation of SMA. Intersection of the two curves specifies the optimum value of SMA incorporation percentage which is equal to 64%. Taking a closer look at the curves indicates that for quantities less than 50% of SMA incorporation, the recentering is relatively constant while dissipated energy sustains a drastic decrement. Therefore, it is deduced that due to high unitary cost of SMAs, the devices with lower portion of SMA have an adverse effect in terms of optimum performance. It is interesting to note that the definition of the optimum point depends on the design performance level.

4. Five-story benchmark building equipped with hybrid device

A five-story building with inverted V bracing system equipped with hybrid SMA-steel devices performing as an eccentrically braced frame (EBF) is designed for a site which claims to be a very high seismic zone (Tehran, Iran). A numerical study is conducted to evaluate the proficiency of the hybrid device in response mitigation. The structure is supposed to be located on soil type C (average shear wave velocity to a depth of 30-m would be 180-360-m/s). The building is square in plan and consisted of 3 bays of 6m in each direction and the story height of 3.2m as shown in Fig. 8. The structure has been designed according to Iranian Earthquake Resistance Design Code (Standard no. 2800, 2005) and Iranian National Building Code, steel structure design (Iranian national building code, part 10, 2006). It is worth noting that hybrid device is designed with the purpose of restricting the interstory drifts. So, the frame yielding is certainly prevented; main structural members will remain in elastic range as a result of capacity design principle. Gravity loads of 6 KN/m² and 2 KN/m² are considered for dead and live loads, respectively.

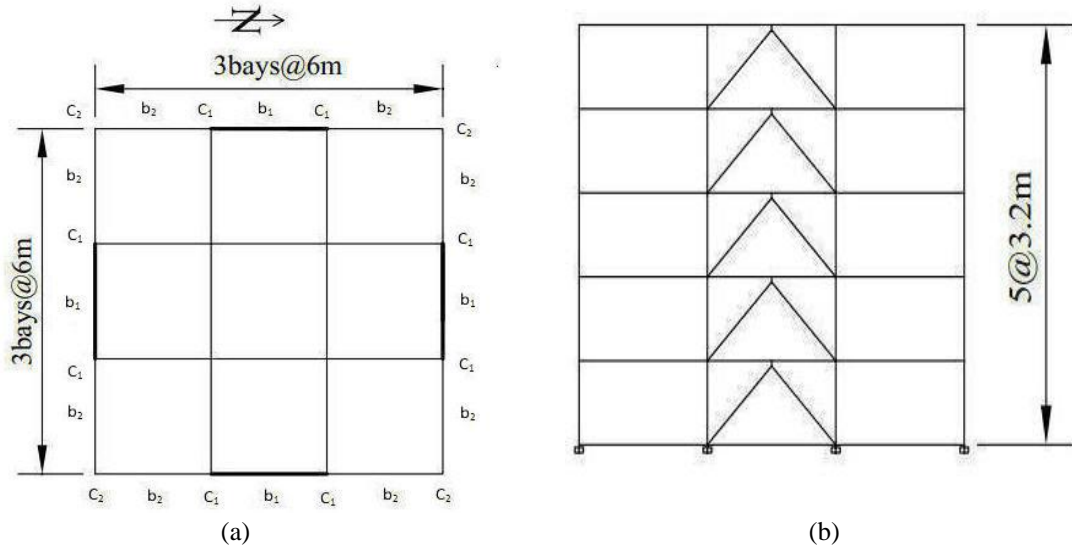


Fig. 8 Configuration of the model structure (a) Plan of the structure (b) Elevation of the controlled structure

Table 2 Mechanical properties of designed devices for each story

Story Level	L_{pipe} (mm)	t_{pipe} (mm)	A_{SMA} (mm ²)
1	300	7.15	2200
2	300	6.6	2053
3	300	6.8	1408
4	300	8.5	-
5	300	4.7	-

4.1 Concept and design of hybrid device

In order to design the wire section of the hybrid device, different values of incorporation percentage of SMA are assigned to each story level. These selections are based on the restrictions of pipe design. The thickness of the pipe will be thin as a result of high incorporation percentage of SMA; this will contribute to intense possibility of buckling. So, the incorporation percentage of 50%, 50% and 40% are chosen for the first, second and third story, respectively. As mentioned, due to smaller values of story shear which leads to thinner thicknesses of the pipes, the fourth and fifth stories have no SMA wires. The length of the pipe is considered to be 0.3m for all stories. It is worth mentioning that the lower quantities for this parameter cannot satisfy the ductility of the frame. The radius of the pipe is selected in such a way that its performance remains in shear range, since more ductility can be found in the shear links compared to the flexural ones. For all the steel members, the yield strength is equal to 240MPa. Properties of designed steel pipes and SMA wires are listed in Table 2.

4.2 Design of frame elements

Braces of EBF frame should be designed for combined axial and flexural forces; consequently,

Table 3 Cross sections for the members of controlled structure

Story	C_1	C_2	b_1	b_2	Brace
1	TUBO 300×300×30	TUBO 150×150×12	HEB 300	HEB 200	TUBO 200×200×20
2	TUBO 300×300×30	TUBO 150×150×12	HEB 300	HEB 200	TUBO 200×200×20
3	TUBO 200×200×20	TUBO 150×150×10	HEB 300	HEB 200	TUBO 200×200×20
4	TUBO 200×200×20	TUBO 150×150×10	HEB 300	HEB 200	TUBO 200×200×14
5	TUBO 200×200×20	TUBO 150×150×10	HEB 300	HEB 200	TUBO 200×200×14

Table 4 Cross sections for the members of uncontrolled structure

Story	C_1	C_2	b_1	b_2	Brace
1	TUBO 240×240×35	TUBO 100×100×10	HEB 240	HEB 200	TUBO 140×140×14.2
2	TUBO 240×240×35	TUBO 100×100×10	HEB 240	HEB 200	TUBO 140×140×14.2
3	TUBO 160×160×17.5	TUBO 80×80×10	HEB 240	HEB 200	TUBO 140×140×14.2
4	TUBO 160×160×17.5	TUBO 80×80×10	HEB 240	HEB 200	TUBO 120×120×12.5
5	TUBO 160×160×17.5	TUBO 80×80×10	HEB 240	HEB 200	TUBO 120×120×12.5

bracing system is assumed to be continuous. According to the AISC (seismic provisions, 2005), strain hardening and material uncertainties cause link beams to develop larger shear strength than nominal shear strength. Maximum shear capacity of the link beam is $V_u = \Omega * R_y * V_n$, V_n is the nominal plastic shear capacity. For brace members an overstrength factor of Ω has been given equal to 1.25. R_y is the ratio of the expected yield stress to the minimum yield stress and depends on the type of the steel. Table of R_y values proposes the coefficient of 1.5 for the grade of steel used in this study (A-36).

Due to symmetry of the plan, only one braced frame of the structure is considered. Table 3 lists the members of the five-story braced frame except the hybrid devices; C_1 , C_2 , b_1 and b_2 are shown in Fig. 8(a). Rectangular hollow sections (TUBO) are used for the columns and braces and wide flange sections (HEB) are selected for beams.

For comparison purpose, a concentrically braced frame (CBF) with identical geometry is also designed. Table 4 gives the beams, columns and braces properties of the five-story frame. As can be seen, cross sections of the EBF members are larger than the CBF structure. The main reason relies on the “capacity design” criterion. The intent of this rule is to assure that yielding in an EBF occurs in the links; the columns, braces and beam segments outside of the link must be designed to resist the loads developed by the yielded link. Based on the capacity design principle, the nominal shear strength of the link V_n is increased by two mentioned factors (Ω and R_y); this leads to larger member sections. It should be mentioned that due to favorable performance of EBF systems, economical construction is neglected to mitigate the cost of damages.

5. Time history analysis of 5 story buildings

2D numerical model of the frame with the hybrid device was developed using ABAQUS programming. Three element types are applied to model the different parts of the frame; shell, beam and truss elements. Due to only axial forces being applied in the SMA wires, a single truss element is used to model each recentering component.

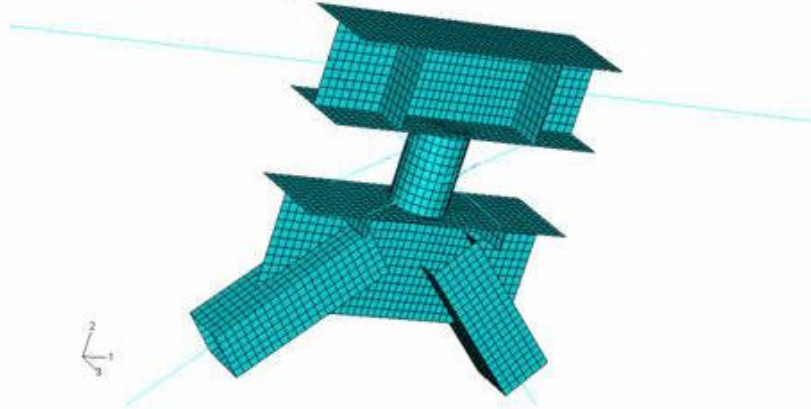


Fig. 9 Details of the hybrid device in numerical modeling

Fig. 9 depicts the sections modeled using shell, beam and truss elements. As mentioned, parts of the structure with axial performance include SMA wires are modeled by truss elements. Besides, beam elements are considered for braces, beams and columns. The whole part of the hybrid device and some sections of adjacent members which have the possibility of nonlinear deformations are modeled using shell elements. These parts are finely meshed to demonstrate the plastic deformations of the device, as shown in Fig. 9. In order to connect shell and beam elements, kinematic coupling is defined between a control point which is the end point of the beam element and lines which form the shell element surface. Through this method, the control point will determine the deformations of the shell slave surface. The points which connect these two different elements are coupled in all six degrees of freedom to unify their behaviors. As a result of three translational degrees of freedom in truss elements, the connection point between the truss and shell elements is constrained in only three translational degrees of freedom.

The outward bulging in bottom flange of the beam and the rotation of device bottom plate are probable as a result of unbalanced forces induced in the device. Therefore, two identical stiffeners are placed in the beam. In addition, same stiffeners are accommodated at the nether of the device bottom plate. It should be noted that the selection of pipe section with its high lateral torsional buckling strength as a dissipater component would prevent the probability of out-plane buckling.

An implicit FE analysis has been performed using ABAQUS/Standard; after each increment the analysis uses Newton-Raphson iterations to enforce equilibrium of the internal structure forces with the externally applied loads. This type of analysis is more accurate and takes slightly larger increment steps. Besides, the Newmark-beta integration method is used to solve the dynamic equations. Effect of geometric non-linearity originated from large displacements is considered using “nlgeom” activation in ABAQUS analyses.

In order to determine the capability of the device in reducing the residual displacements of the frame, free vibration step of 10s is defined after the end of the earthquake; all nodes of the base are prevented from moving in X-direction.

5.1 Record selection

Five ground motion records are used for time history analyses of both controlled and

Table 5 Characteristics of ground motion records

Event	Soil	M_w	PGA (g)	Duration (s)
Loma Prieta, 1989	C	6.9	0.529	39.95
Tabas, 1978	C	7.4	0.836	32.82
Kobe, 1995	C	6.9	0.611	40.95
Northridge, 1994	C	6.7	0.897	39.995
Imperial Valley, 1979	C	6.5	0.707	38.955

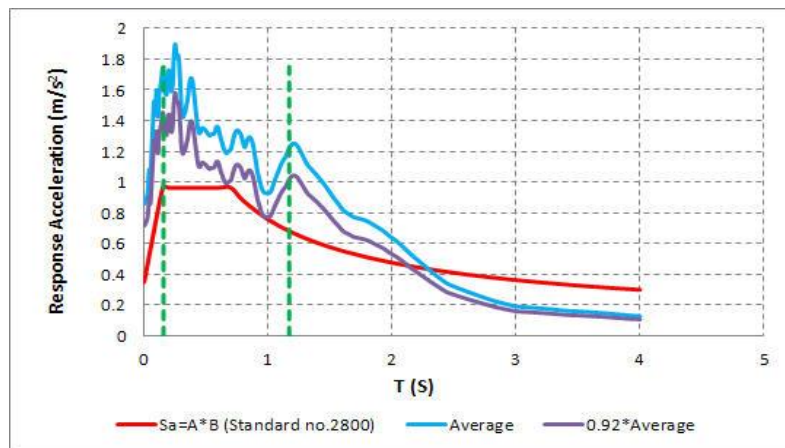


Fig. 10 Average and design response spectra

uncontrolled structures. Appropriate ground motions should be selected from the events having magnitudes, fault distance and source mechanisms which are consistent with the maximum considered earthquake. These records include 1989 Loma Prieta, 1978 Tabas, 1995 Kobe, 1994 Northridge and 1979 Imperial Valley earthquakes. The ground motions belong to a set of earthquake of relatively large magnitudes (M_w) on soil type C, as listed in Table 5.

The selected records are scaled according to the Iranian Earthquake Resistance Design Code (Standard no. 2800). The spectra of the records with 5% damping are determined. An average of the obtained spectra is determined and named as “average spectrum”. The “scale factor” is obtained such that the value of the 5% damped average spectrum should not be less than the design response spectrum in the range of $0.2T$ to $1.5T$, where T is the dominant period of the structure. As can be seen in Fig. 10, the scale factor of 0.92 is obtained. The specified scale factor should be multiplied by each ground motion and used in the dynamic analysis. Fig. 10 shows the design response spectrum and the average of records' response spectra, dashed lines indicate the target period range.

6. Analysis results and discussions

6.1 Structural response

Table 6 shows the elastic stiffness and dominant period of the frames with and without the

Table 6 Effect of hybrid device on stiffness and period of the structure

Frame type	Elastic stiffness (KN/m)	Fundamental period (s)
Controlled	33963	0.78
Uncontrolled	43455	0.64

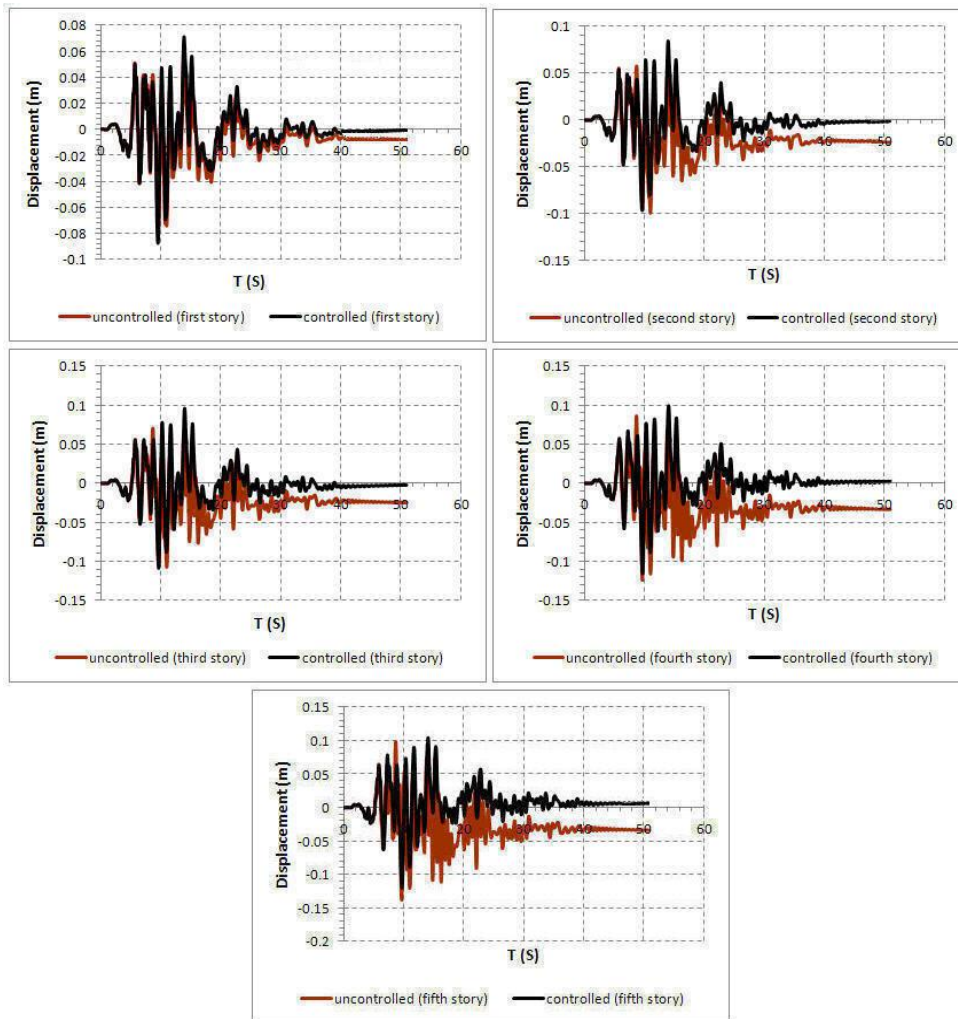


Fig. 11 The Loma Prieta earthquake, time histories of displacement

hybrid device. As evidences, the hybrid device reduces the stiffness and increases the fundamental period.

Figs. 11 and 12 compare the time histories of displacement and acceleration for each floor of the controlled and uncontrolled structures under the Loma Prieta earthquake. The influence of the hybrid device on amelioration of the residual displacement and acceleration response is seen in the figures. The results indicate that the residual displacement of all floors experiences major reduction; this highlights the favorable participation of SMA wires. The acceleration response

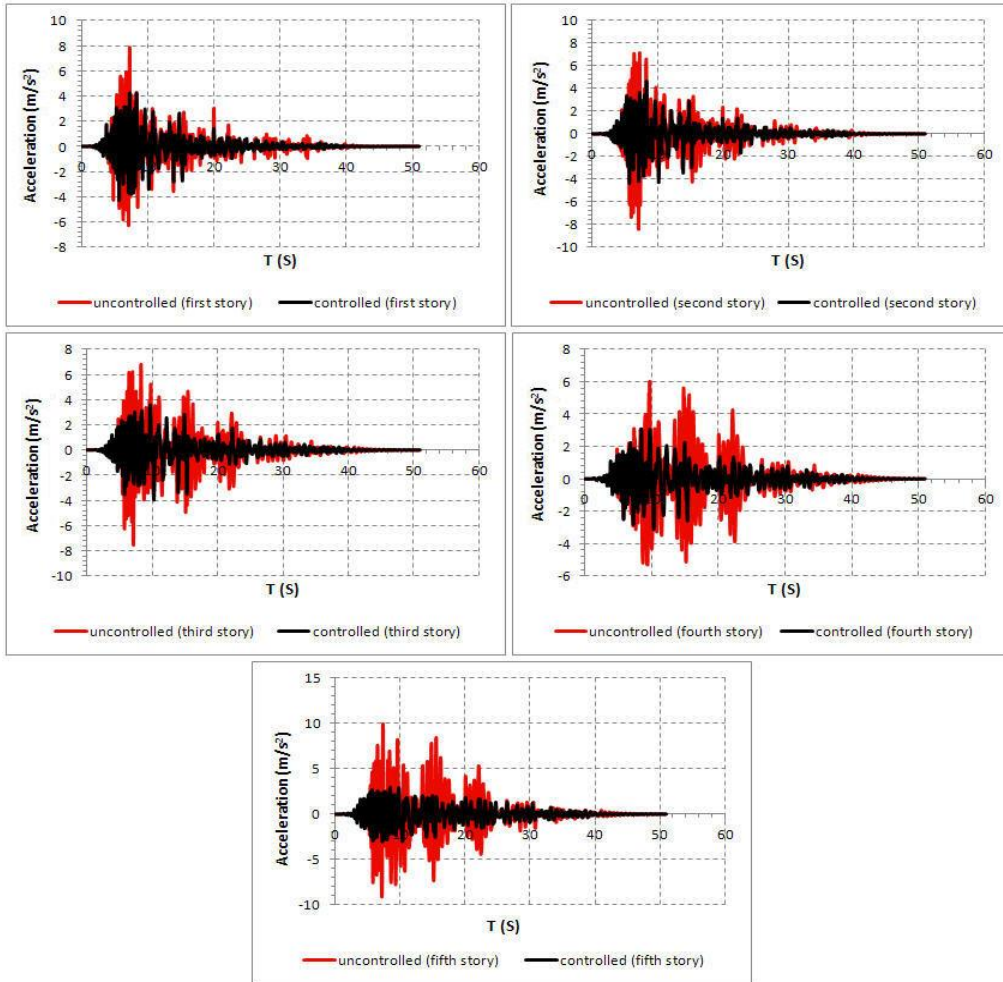


Fig. 12 The Loma Prieta earthquake, time histories of acceleration

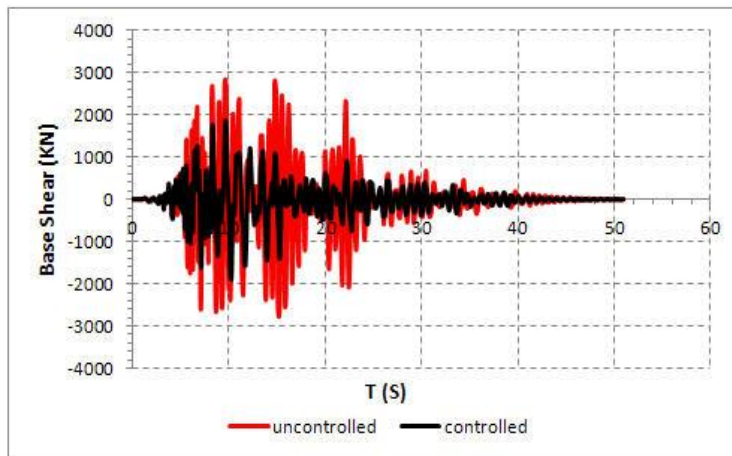


Fig. 13 Base shear response history for controlled and uncontrolled structures (Loma Prieta earthquake).

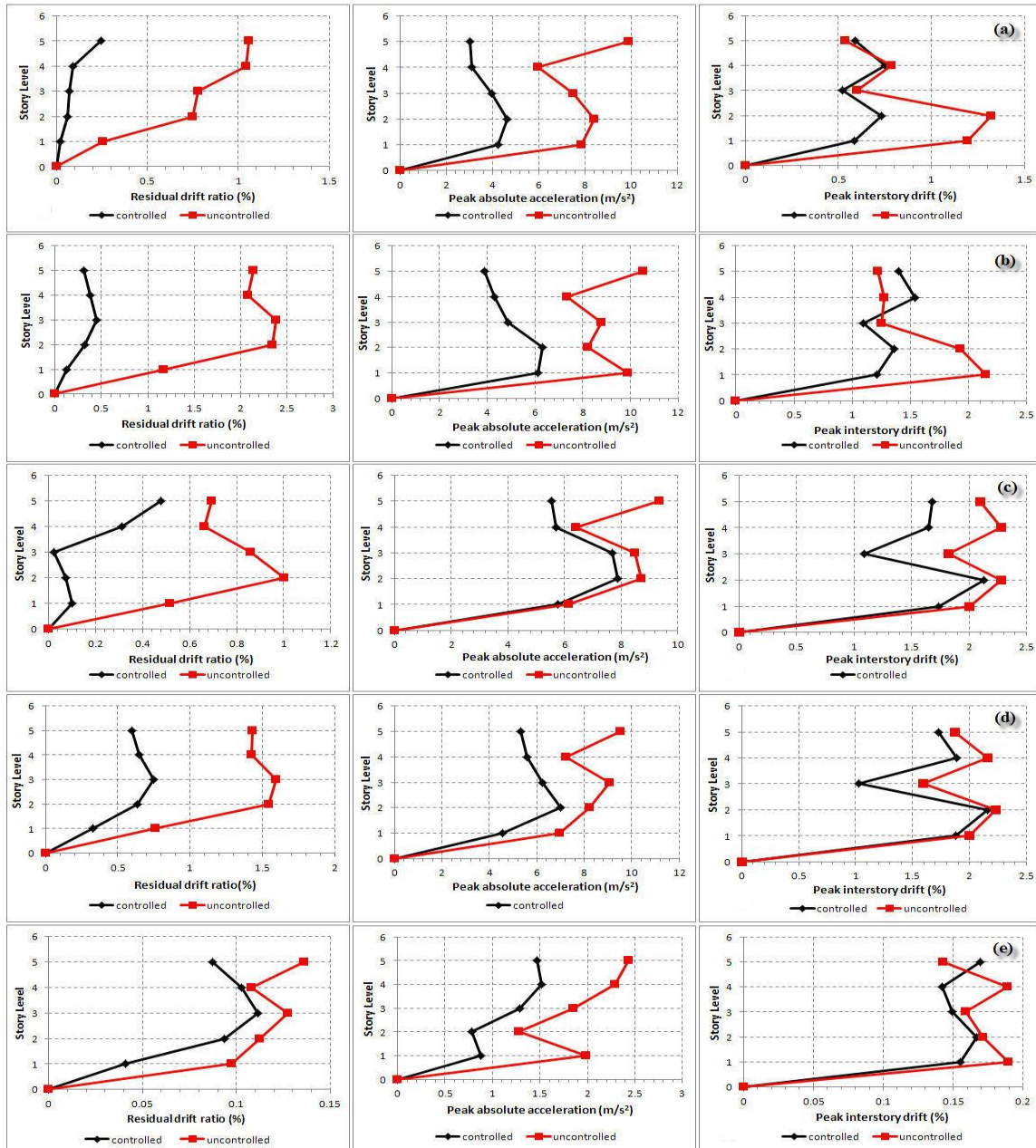


Fig. 14 Profiles of residual drift ratio, peak absolute acceleration and peak interstory drift under (a) Loma Prieta (b) Tabas (c) Kobe (d) Northridge (e) Imperial Valley excitations

during the entire duration of the excitation is smaller for the controlled structure and the main reduction of the absolute acceleration is achieved for the roof story. As can be seen in Fig. 12, the maximum acceleration response is reduced up to 69% for the fifth floor under Loma Prieta excitation.

Fig. 13 provides the time history of base shear for both controlled and uncontrolled structures under the Loma Prieta earthquake as a sample. The result obviously indicates that the peak of the base shear is lower for the structure equipped with the hybrid device. This confirms the favorable shear performance of steel pipe which leads to large amounts of dissipated energy.

Fig. 14 presents the profiles of residual drift ratio, peak absolute acceleration and peak interstory drift for controlled and uncontrolled frames. Residual drift ratio is defined as the ratio of the residual displacement to the corresponding story height. As can be seen, peak acceleration and peak interstory drift of the controlled frame are reduced in comparison with the uncontrolled frame. The lack of SMA wires is observed in the interstory drift profiles of Tabas and Imperial Valley earthquakes for the fourth and fifth floors.

In addition to the interstory drift and peak absolute acceleration responses which are significant parameters to define the operation of the structure, the residual drift ratio is a noteworthy factor in estimating the after-earthquake vulnerability of the structure. As shown in Fig. 14, the hybrid device is very effective in suppressing the residual drift ratio for all excitations. This is due to the recentering property of the SMA wires, which creates a flag-shaped hysteresis loop. As mentioned before, self-centering is a promising trait of SMA to reduce or even eliminate the permanent structural deformation. The residual drift ratio is reduced up to 97%; the maximum reduction occurred at the third floor of the structure under the Kobe earthquake.

6.2 Energy consideration

This section is dedicated to specify the potential of the hybrid device in attenuation of the input energy. The specific amount of energy induced to the structure is transformed to the other energy modes as strain and plastic energy. So, the quantity of energy which is dissipated by means of structural deformations could be beneficial to design the hybrid control systems. Fig. 15 reveals that the main origin of dissipation is the steel pipe. The figure shows the amounts of earthquake input energy and dissipation by the whole model, steel pipe and SMA wires.

As shown in the figure, SMA wires have negligible contribution in energy dissipation in comparison with the steel pipe; it is obvious due to their small cross sectional area. The input energy is mainly dissipated by the plastic deformation of the steel pipe. Comparison between the results shows that the steel pipe has a better performance under the Tabas excitation (46% absorption from the input energy). The absorbed energy due to the pipe and connections elastic deformation is the secondary source of dissipated energy.

It should be noted that due to higher duration of the Kobe earthquake, it has the larger amount of input energy.

7. Conclusions

The paper proposed an innovative hybrid device for seismic protection of structures subjected to five major earthquakes. In the hybrid device, which indicated a double flag-shaped hysteresis loop, SMA wires were used as recentering components while energy absorption of the device was supplied by the steel pipe. The incorporation percentage of SMA was the most important factor that influenced the hysteresis loop. An optimum percentage of 64% was obtained for this parameter through the evaluation of several devices behavior.

A five-story braced frame was designed with hybrid device installed between the beam and

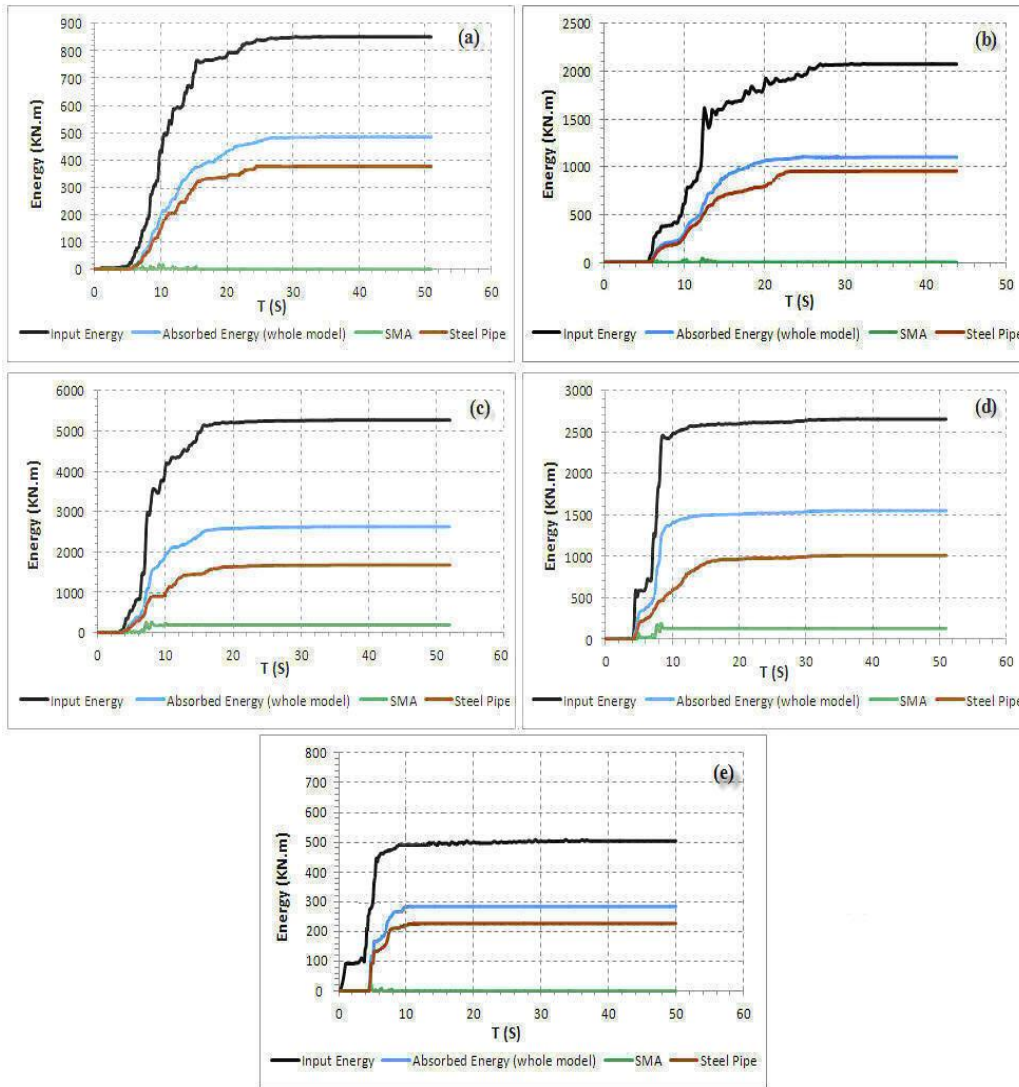


Fig. 15 Time histories of energy absorption for (a) Loma prieta (b) Tabas (c) Kobe (d) Northridge (e) Imperial Valley excitations

chevron braces. The design of structural members was performed based on capacity design rule. A comparative study with both the controlled and uncontrolled structures was conducted to indicate the workability of the hybrid device in amelioration of the residual drift ratio, peak absolute acceleration, peak interstory drift and the base shear. Maximum reduction of 97%, 69% and 51% was observed in residual drift ratio (Kobe), peak absolute acceleration (Loma Prieta) and peak interstory drift (Loma Prieta), respectively.

Although the results of this article suggest promise for implementing the SMA-based hybrid device, further studies are still necessary to confirm the numerical results experimentally.

Acknowledgements

Financial Support by the Iranian National Science Foundation (INSF), grant No. INSF 91004065 is gratefully acknowledged.

References

- ABAQUS Version 6.5, Hibbitt, Karlsson & Sorensen, Inc., Pawtucket, RI.
- AISC (2005), American Institute of Steel Construction, Seismic provisions for structural steel buildings, Chicago.
- Asgarian, B. and Moradi, S. (2011), "Seismic response of steel braced frames with shape memory alloy braces", *J. Constr. Steel Res.*, **67**, 65-74.
- Asgarian, B. and Shokrgozar, H. D. (2009), "BRBF response modification factor", *J. Constr. Steel Res.*, **65**(2), 290-298.
- Asgarian, B. and Amirhesari, N. (2008), "A comparison of dynamic nonlinear behavior of ordinary and buckling restrained braced frames subjected to strong ground motion", *Struct. Des. Tall Special Build.*, **17**(2), 367-386.
- Constantinou, M.C., Soong, T.T. and Dargush, G.F. (1998), "Passive energy dissipation systems for structural design and retrofit", Research Foundation of the State University of New York and Multidisciplinary Center for Earthquake Engineering Research, Buffalo NY.
- DesRoches, R., McCormick, J. and Delemont, M. (2004), "Cyclic properties of superelastic shape memory alloy wires and bars", *J. Struct. Eng.*, ASCE, **130**, 38-46.
- Dolce, M., Cardone, D. and Marnetto, R. (2000), "Implementation and testing of passive control devices based on shape-memory alloys", *Earthq. Eng. Struct. Dyn.*, **29**, 945-968.
- Dolce, M. and Cardone, D. (2001), "Mechanical behavior of shape memory alloys for seismic applications. 2: austenite NiTi wires subjected to tension", *Int. J. Mech. Sci.*, **43**, 2657-2677.
- Dolce, M. and Cardone, D. (2006), "Theoretical and experimental studies for the application of shape memory alloys in civil engineering", *J. Eng. Mater. Technol.*, ASME, **128**(3), 302-311.
- Duerig, T.W., Melton, K.N., Stoeckel, D. and Wayman, C.M. (1990), *Engineering Aspects of Shape Memory Alloys*, Butterworth-Heinemann Ltd, London.
- Fahnestock, L.A., Sause, R. and Ricles, J.M. (2003), "Analytical and experimental studies on buckling restraint braced composite frames", *Proceedings of the International Workshop on Steel and Concrete Composite Construction (IWSCCC)*, NCREC, Taipei, Taiwan.
- Iranian Code of Practice for Seismic Resistance Design of Buildings (2005), Standard No. 2800, 3rd Edition, Building and Housing Research Center.
- Iranian National Building Code for Structural Design (2006), Part 10, Ministry of Housing and Urban Development, Tehran, Iran.
- Jalaeefar, A. and Asgarian, B. (2012), "A simple hybrid damping device with energy dissipating and re-centering characteristics for special structures", *Struct. Des. Tall Spec. Build.*, **23**, 483-499.
- Janke, L., Czaderski, C., Motavalli, M. and Ruth, J. (2005), "Applications of shape memory alloys in civil engineering structures-overview, limits and new ideas", *Mater. Struct.*, **38**(5), 578-592.
- Karavasilis, T.L., Blakeborough, T. and Williams, M.S. (2011), "Development of nonlinear analytical model and seismic analyses of a steel frame with self-centering devices and viscoelastic dampers", *Comput. Struct.*, **89**, 1232-1240.
- Karavasilis, T.L., Keralala, S. and Hale, E. (2012), "Hysteretic model for steel energy dissipation devices and evaluation of a minimal-damage seismic design approach for steel buildings", *J. Constr. Steel Res.*, **70**, 358-367.
- Maleki, S. and Bagheri, S. (2010), "Pipe damper, Part I: experimental and analytical study", *J. Constr. Steel Res.*, **66**, 1088-1095.

- Marshall, J. and Charney, F. (2010), "A hybrid passive control device for steel structures, I: development and analysis", *J. Constr. Steel Res.*, **66**, 1278-1286.
- Miyazaki, S., Imai, T., Igo, Y. and Otsuka, K. (1986), "Effect of cyclic deformation on the pseudoelasticity characteristics of Ni-Ti alloys", *Acta Metall.*, **17**, 115-120.
- Motahari, S.A., Ghassemieh, M. and Abolmaali, S.A. (2007), "Implementation of shape memory alloy dampers for passive control of structures subjected to seismic excitations", *J. Constr. Steel Res.*, **63**, 1570-1579.
- Ozbulut, O.E. and Hurlbauss, S. (2011), "Re-centering variable friction device for vibration control of structures subjected to near-field earthquakes", *Mech. Syst. Sig. Proc.*, **25**, 2849-2862.
- Sabelli, R., Mahin, S. and Chang, C. (2003), "Seismic demands on steel braced frame buildings with buckling restrained braces", *Eng. Struct.*, **25**(5), 655-666.
- Sabol, T.A. (2004), "An assessment of seismic design practice of steel structures in the United States since the Northridge earthquake", *Struct. Des. Tall Spec. Build.*, **13**(5), 409-423.
- Song, G., Ma, N. and Li, H.N. (2006), "Application of shape memory alloys in civil structures", *Eng. Struct.*, **28**(9), 1266-1274.
- Tagawa, H. and Gao, J. (2012), "Evaluation of vibration control system with U-dampers based on quasi-linear motion mechanism", *J. Constr. Steel Res.*, **70**, 213-225.
- Tremblay, R., Archambault, M.H. and Filiatrault, A. (2003), "Seismic performance of concentrically braced steel frames made with rectangular hollow bracing members", *J. Struct. Eng.*, **129**(12), 1626-1636.
- Tremblay, R. and Poncet, L. (2004), "Improving the seismic stability of concentrically braced steel frames", *Proceedings of the 2004 SSRC Annual Technical Session and Meeting*, Long Beach, Calif.
- Uang, C.M. and Kiggins, S. (2003), "Reducing residual drift of buckling-restrained braced frames", *Proceedings of the International Workshop on steel and Concrete Composite Construction, National Center for Research on Earthquake Engineering*, National Taiwan Univ, Taiwan. Paper No. 18.
- Uriz, P. and Mahin, S. (2004), "Seismic performance assessment of concentrically braced steel frames", *Proceedings of the 13th World Conf on Earthquake Engineering, Canadian Association for Earthquake Engineering (CAEE)*, Vancouver, Canada, August, Paper No. 1639.
- Van Humbeeck, J. (1991), "Cycling effects, fatigue and degradation of shape memory alloys", *J. Phys.*, **4**, 189-197.
- Wada, A. (2010), "Seismic design for resilient society", *Proceedings of the 7th International Conference on Urban Earthquake Engineering and 5th International Conference on Earthquake Engineering*, Tokyo, March.
- Watanabe, A., Hitomi, Y., Saeki, E., Wada, A. and Fujimoto, M. (1988), "Properties of brace encased in buckling-restraining concrete and steel tube", *Proceedings of the 9th World Conference on Earthquake Engineering, International Association for Earthquake Engineering (IAEE)*, Tokyo-Kyoto, Japan, August.
- Yang, W., DesRoches, R. and Leon, R.T. (2010), "Design and analysis of braced frames with shape memory alloy and energy-absorbing hybrid devices", *Eng. Struct.*, **32**, 498-507.